Chapter 5

Multifunctional Behavior in Double Perovskite

EuPrCoMnO$_6$

5.1 Introduction

The increasing demand of technology for energy devices requires the growth of high-performance materials. Such materials should come up with some novel characteristics which can be put up with long-term services even in severe environments [126,128,244–246]. The possessing of electric and magnetic orders simultaneously has been of prime interest for their potential applications for next-generation electronic devices [244–246]. In this aspect, a class of material known as double perovskite (DP), $A_2BB'O_6$ (where A: rare-earth ions; B, B': transition metal ions) has been much investigated owing to their various charismatic properties like multiferroicity, spin-phonon coupling, cationic ordering, colossal magneto-resistance, and magneto-capacitance, etc [47,49,51,247,248]. These compounds mostly crystallize either in a disordered orthorhombic structure with space group Pbnm or in an ordered monoclinic structure with space group P21/n [248]. The ordered DPs mainly show ferromagnetism (FM) via B^{2+}-O-B'^{4+} super-exchange interaction [47]. However, there is always possible that in the ordered state itself few B and B' cations swap out their crystallographic positions, thus introducing anti-site disorder (ASD) [51,247] which may prompt additional anti-ferromagnetic (AFM) interactions within the system in the form of B^{2+}-O-B^{2+} or B'^{4+}-O-B'^{4+} and hence weakens the FM. The ASD also has profound effects on the many physical properties of DPs, especially the magnetic properties and can lead to fascinating phenomena like exchange bias, low-temperature spin-glass states, room temperature giant magneto-dielectricity, etc [140,249].

In DPs substitutions of different A-site cations modifies the B-O-B' bond angle and length. Consequently, transition temperature changes and leads to an inhomogeneous magnetic

ground state by means of multiple magnetic interactions build up in the system. The same has been reported in numerous perovskites in the form of clustered phase or Griffiths-like-phase (GP) where unusual magnetic state of short-range FM clusters of different sizes appears just above transition temperature (T_C) up to a certain temperature T_{GP} [49,67,247]. However, when a system has multiple magnetic phases, an exchange bias (EB) will appear owing to the formation of the unidirectional FM exchange anisotropy at the interfaces of two different magnetic phases [250,251]. The EB effect is very important phenomenon for the technological purpose as it is tremendously useful in giant magneto-resistive random access memory devices, read-heads in magnetic recording, in permanent magnets and in stabilizing nanoparticles etc. These interesting phenomena give the idea to elaborate the magnetic property of DPs much more.

Additionally, the existence of II-type of ferroelectricity, driven by magnetostriction has been observed in DPs A_2CoMnO_6 due to breaking of inversion symmetry by means of distortion of ferro/antiferro bonds similar to observed ferroelectricity in Ca_3CoMnO_6 [63,78,141,170,252]. The ferroelectric and magnetic transition in DPs Lu_2CoMnO_6 and Y_2CoMnO_6 occurs at the same temperature ~35 K and 80 K respectively while its origin has been supposed to be the same as Ca_3CoMnO_6 [63,78,141]. Though the structures of DPs are much different than the Ca_3CoMnO_6, particularly the second-nearest-neighbor Co-Co/Mn-Mn distances are much larger in A_2CoMnO_6 than that of Ca_3CoMnO_6. Thus, the strength of exchange interactions in the two systems will be different. Earlier, Jia et. al. has performed theoretical study using the first-principle calculations to see the origin of ferroelectricity and magnetic ordering [253]. They found that the spin ordering originates due to a subtle competition between the ferromagnetic Co-O-Mn super-exchange and antiferromagnetic Co-

Mn direct-exchange interaction along particular c-axis. So, we are highly motivated to investigate magnetic and dielectric studies of similar DPs.

The previous study of many DPs with "A" site non-magnetic ions like La, Y, Lu, Eu has drawn extensive attention as they exhibit most exciting feature in the isothermal magnetization curve i.e., meta-magnetic-transition (MMT) [5,120–122,211]. In this chapter, we have chosen a DP system, such that 50% of A-site is occupied by non-magnetic ions and that of other 50% by magnetic ions i.e., $EuPrCoMnO_6$ (EPCMO). We have reported magnetic properties and the reason behind it of one of the end members Eu_2CoMnO_6 (ECMO) in our earlier investigation [211]. It has been observed that ECMO has much attention-grabbing property viz. MMT, spin-phonon coupling wide band-gap, GP, etc. However, other end member Pr_2CoMnO_6 (PCMO) has been investigated somewhere else [67]. PCMO also has fascinating physical properties like double FM transitions, GP, strong spin-phonon coupling effect, EB, etc. Thus, the incorporation of ECMO and PCMO together may lead to some extraordinary behavior. In the present manuscript, we have reported the coexistence of giant dielectric constant, different magnetic phases and strong magneto-resistance in EPCMO suggesting this material as a multi-functional material.

5.2 Experimental

The polycrystalline pellets of DP sample EPCMO were prepared via solid-state reaction route as described elsewhere [211], where highly pure oxides Eu_2O_3, Pr_6O_{11}, CoO and Mn_2O_3 were used as starting material. The XRD pattern of the powdered sample was collected using a Rigaku Miniflex-II powder diffractometer. The XRD pattern was analyzed with Fullprof software using Rietveld method. The magnetic properties were measured via a

quantum design MPMS3 (magnetic property measurement system), which is a SQUID (superconducting quantum interference device) magnetometer. Dielectric and impedance measurements were carried out using a highly sensitive Keysight E4980A Precision LCR meter with a He-cooled CCR (closed-cycle refrigerator). The electrical DC resistivities without and with magnetic field were measured with a Keithley 6517B Electrometer and CCR using the standard 2-probe method.

5.3 Result and discussion

5.3.1 Structural analysis
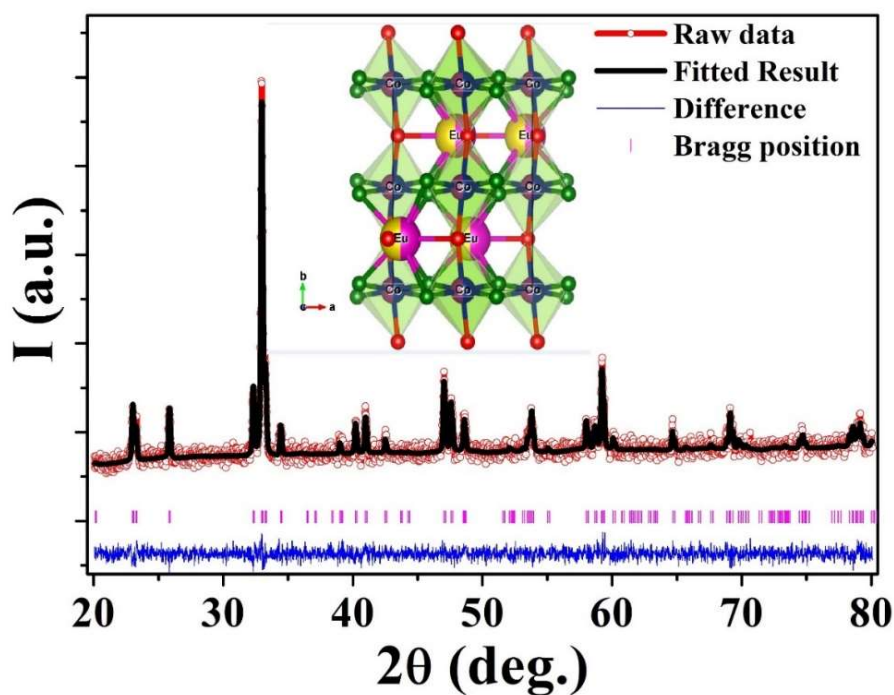
Figure 5.1: *The X-ray diffraction pattern of EPCMO taken at room temperature with inset showing the 3D structure of EPCMO.*

Table 5.1: *Structural parameters extracted from refinement of EPCMO at room temperature.*

Parameters/Space group	Pnma (62)
a	5.53891 Å
b	7.63968 Å
c	5.38782 Å
V	227.9880 Å^3
Eu/Pr site	4c
x	0.05244
y	0.25000
z	-0.01461
Co site	4b
x	0.00000
y	0.00000
z	0.50000
Mn site	4b
x	0.00000
y	0.00000
z	0.50000
O(1) site	4c
x	0.46520
y	0.25000
z	0.11018
O(2) site	8d
x	0.25827
y	0.03114
z	0.71634
Chi^2	3.46
R_p	5.13
R_{wp}	6.45
R_{exp}	3.47
GoF-Index	1.9

Fig. 5.1 is showing the XRD pattern of EPCMO along with Rietveld refinement. The XRD pattern of powdered EPCMO was best refined in a disordered orthorhombic phase with space group *Pnma* where Co/Mn are randomly distributed over B-sites similar to its parent system [254]. The inset of Fig. 5.1 consists of a 3D structure of EPCMO showing the distribution of atoms over its site, visualized using VESTA [255]. The crystallographic data of EPCMO have been tabularized in Table 5.1.

5.3.1 Magnetic study

Fig. 5.2 (a) shows the temperature-dependent ZFC and FC induced magnetization (M) of EPCMO at 100 Oe field. Magnetization varies very slowly down to 160 K. However below 160 K, M(T) increases and shows two successive magnetic transitions in the vicinity of T_{C1} ~146 K and T_{C2} ~138 K. The dM/dT curve also exhibits inflection points at these transition temperatures (as shown in the inset of Fig. 5.2(a)). Based on literature of A_2CoMnO_6 DP'S, this transition around ~146 K is credited to the FM ordering of Co^{2+}-O-Mn^{4+} super-exchange interactions while second transition ~138 K arises either due to the Co^{3+}-O-Mn^{4+} super-exchange FM interactions or related to existence of few of Co^{3+} and Mn^{3+} in the disordered phase along with the dominant FM interactions arising from the ordering of Co^{2+} and Mn^{4+} ions [49,67,256]. FM transition temperature of EPCMO is in good agreement as it is higher than the parent system ECMO and is less than that of PCMO, as the size of Pr^{3+} ion is higher than Eu^{3+} ion. Transition temperature of A_2CoMnO_6, increase linearly for different A (rare-earth ion) from 48 K for Lu_2CoMnO_6 to 204 K for La_2CoMnO_6, as their ionic size increases from Lu to La [54]. It is important to mention here that even in an ordered system, few of the Co/Mn exchanges their crystallographic positions, thus leading to anti-site disorder (ASD).

ASD activates supplementary AFM ordering through Co^{2+}-O^{2-}-Co^{2+} and Mn^{4+}-O^{2-}-Mn^{4+} super-exchange interactions. The decreasing nature of M in ZFC curves below ~133 K (T_a) has been attributed to the multifarious relationship of magnetic interaction between rare earth and transition metal sub-lattices [47,49]. The cusp temperature T_a is a point where local magnetic anisotropy energy and the external magneto-static energy acquire balanced. The huge bifurcation between ZFC & FC curves indicates strong spin frustration/spin-glass state due to presence of different competing spin correlations.

Further, to see the evolution of M, with external field strength, we have carried out ZFC/FC magnetization measurements at the different higher applied magnetic field (Fig. 5.2b). The magnetic transition temperature T_{C1} of EPCMO moves toward higher temperature at high magnetic field similar to parent ECMO [211]. This characteristic is attributed to increased spin-order of FM materials at a higher temperature under the influence of high external magnetic field [211,257]. The magnitude of bifurcation between the ZFC/FC curves initially increases
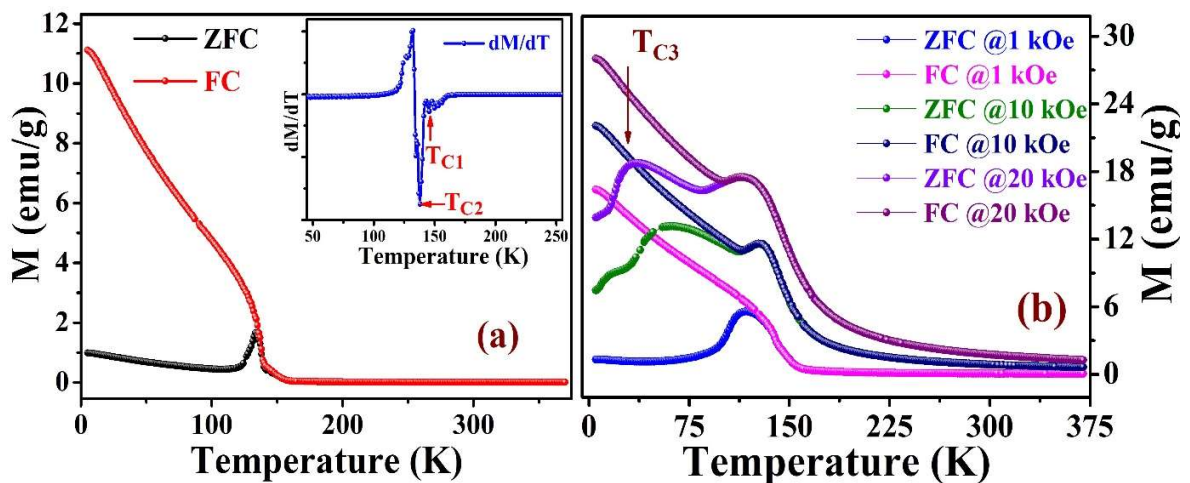
Figure 5.2: *(a) The ZFC/FC magnetization of EPCMO at 100 Oe applied field with inset showing dM/dT curve. (b) The ZFC/FC magnetization of EPCMO at higher applied fields.*

on increasing applied field strength up to 10 kOe and then decreases at higher field. The bifurcation between ZFC and FC M(T) curves is usual in most of the FM materials, which originates due to magnetic anisotropy. Thus, the bifurcation should appear at a lower temperature in a higher magnetic field, which has been observed in EPCMO (Fig. 5.2b) and ECMO [211] as well, due to the suppression of the magnetic anisotropy in high field [257]. Further, the observed cusp in the ZFC-magnetization curve around T_a has suppressed on increasing field, this is a typical signature of the existence of some AFM phases or anti-phase regions in the system. Other than this a third magnetic transition has been observed in EPCMO at high field below 40 K (T_{C3}). This magnetic anomaly has been better described with the help of AC susceptibility spectrum, which is discussed later on.

From the Fig. 5.3, it has been observed that the inverse DC susceptibility (χ^{-1}) curve of EPCMO shows linear behavior above 168 K; confirming a pure paramagnetic state. This data could be fitted by Curie–Weiss (CW) law given by equation $\chi = C/(T - T_{CW})$. The fitting (for
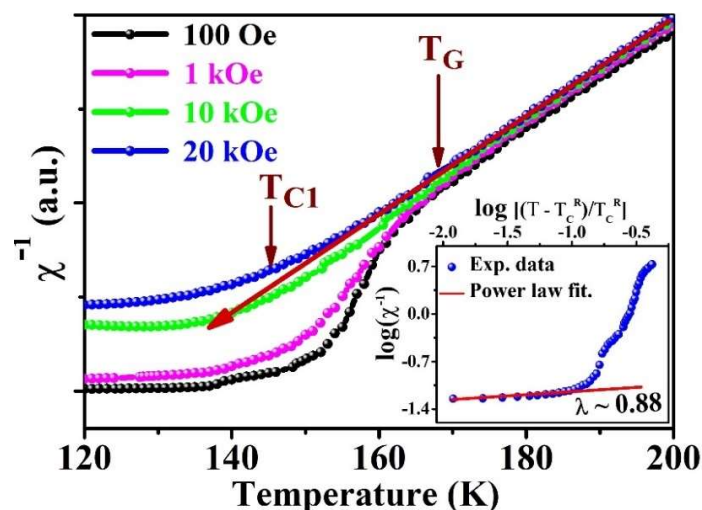
Figure 5.3*: The inverse DC susceptibility vs. temperature at different applied fields of EPCMO with inset showing power law fitting.*

T > 200 K) gives Curie-Weiss temperature (T_{CW}) around +118.6 K, again supporting a leading

ferromagnetic phase. The large difference between T_{C1} & T_{CW}, which can't be assigned to

quantum fluctuations rather it occurs owing to frustration through FM and AFM competition

within the system. Further, it has been observed that the χ^{-1} shows a downturn deviation from

the Curie-Weiss line just below ~168 K (T_{GP}) similar to PCMO [67]. Generally, rare-earth

elements develop multiple magnetic interactions in the system, thus causing inhomogeneous

magnetic ground states, in the form of clustered or phase-separated states [8, 10]. One form of

these clustered phases is well known as the "Griffiths like" phase. The GP was originally

proposed for randomly diluted Ising ferromagnets, where a few fractions of the

crystallographic sites can be occupied with spins and rest sites are either vacant or occupied

by some nonmagnetic elements [100]. The Griffiths phase (GP) arises below a characteristic

temperature, known as Griffith's temperature (T_{GP}) and in the region $T_{C1} < T < T_{GP}$ where the

system exhibits an unusual magnetic state due to the formation of short-range FM clusters of

different sizes in the paramagnetic region [49,67,211]. Thus, downturn behavior of $\chi^{-1}(T)$ of

EPCMO might be due to the emergence of the GP or some other FM clustered phase. The

observed downturn significantly was suppressed at higher applied field, suggesting observed

clustered phase is GP. In the GP phase region $\chi^{-1}(T)$ follows the power-law given by,

$$\chi^{-1}(T) = A \left[\frac{T - T_C^R}{T_C^R} \right]^{1-\lambda} \tag{5.2}$$

Where, A is the constant T_C^R is the reduced random critical temperature of randomly distributed

FM cluster and λ is the DC magnetic susceptibility exponent which should lie within 0 to 1 for

$T_C^R < T < T_{GP}$. The value of T_C^R should be chosen in such a way so that equation 5.2 yields

value of λ close to zero in the PM region for T > T_{GP} [105]. Thus, the value of T_C^R will be almost equal to CW-temperature which is determined using CW equation fitting in high temperature PM region. From the slope of the line fit in GP region (as shown in inset of Fig. 5.3), the value of λ for EPCMO was obtained ~ 0.88.

The isothermal magnetization of EPCMO has been collected at 5 K and 300 K, which is presented in Fig 5.4. From the figure, we can see EPCMO has strong FM type hysteresis at 5 K, which did not attain complete saturation even up to 70 kOe applied magnetic field. At 300 K, M(H) curve is completely linear over the whole cycle with almost negligible hysteresis, thus the system is pure PM at this temperature. We also observe clear steps in the isothermal magnetization curve (i.e., meta-magnetic-transition) at 5 K in third quadrant (around -5 kOe and -10 kOe) and a mirror image was observed in fourth quadrant (around 5 kOe and 10 kOe) as has been demonstrated in the inset of Fig 5.4. Jumps in magnetization occurs only while forward field sweep direction i.e., for 0 to -70 kOe and are absent in decreasing field from -70 to 0 kOe owing to slow spin relaxation and again re-appear in subsequent forward field direction i.e., for 0 to 70 kOe; followed by large hysteresis. However, unlike ECMO, EPCMO has larger step size (ΔM) at high field side (~10 kOe) than the step size at low field side (~5 kOe). Thus, observed MMT in EPCMO are purely field-induced due to transition to a FM state from uncompensated AFM states [258]. In Ca_3CoMnO_6, it has been investigated that the spin flop transition from E*-type magnetic structure ($\uparrow\uparrow\downarrow\downarrow$) to the $\uparrow\uparrow\uparrow\downarrow$ Mn^{4+} (high spin S = 3/2) at first jump and to $\uparrow\uparrow\uparrow\uparrow$ with Co^{2+} (low spin S = 1/2) spin flop at second jump is the possible reason behind sharp step [171]. However, for EPCMO, step size (ΔM) is much smaller, thus, the possibility of field-induced spin flop behind the origin of MMT can be ruled out. Additionally, a close view of M(H) curve shows that the loop is asymmetric around the origin,

indicative of the presence of spontaneous exchange bias (EB), as M(H) loop was recorded in ZFC mode, in EPCMO at low temperature. The magnitude of EB field is given as, $H_{EB} = (H_{C1} + H_{C2})/2$, where H_{C1} and H_{C2} are the magnitudes of magnetic fields at which magnetization becomes zero, which is found to be around 1.17 kOe for EPCMO. The EB mainly appears due to interacting interfaces between FM–AFM magnetic states.
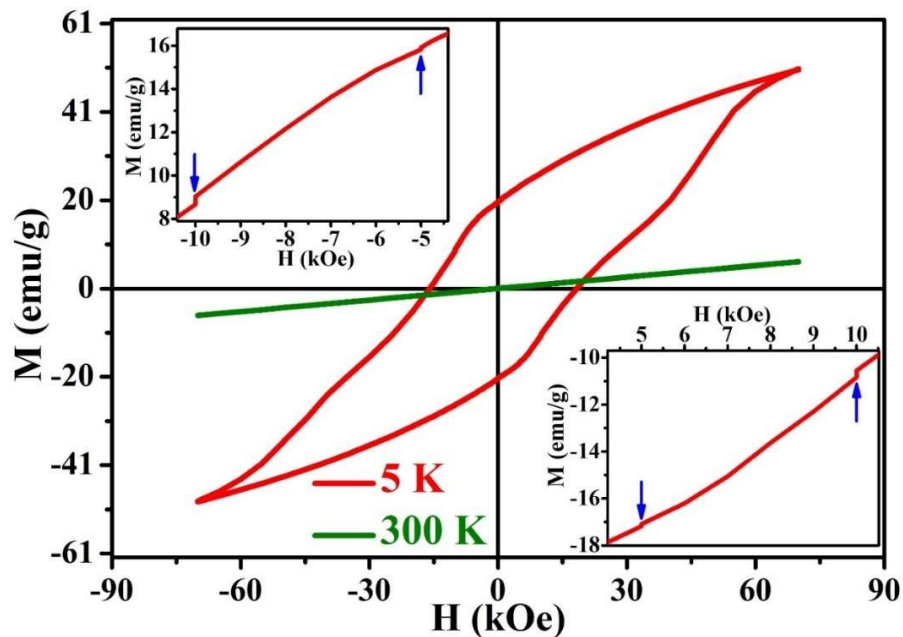
***Figure 5.4**: The isothermal magnetization curves of EPCMO at 5K and 300 K. Inset is showing emergence of metamagnetic transition.*

As seen earlier, bifurcation in ZFC and FC curves is attributed to the existence of superparamagnetic (SPM) state or spin-glass (SG) or cluster-spin-glass (CSG) and is generally observed only in those systems of spin clusters where FC-Magnetization curve displays a cusp around T_a [113]. As, the branching in ZFC-FC M (T) starts ~133 K at low field (100 Oe), shows the existence of high-temperature spin ordering in EPCMO. To explore such dynamics of spin, we have carried out AC susceptibility measurements elaborately. Both, the real part of
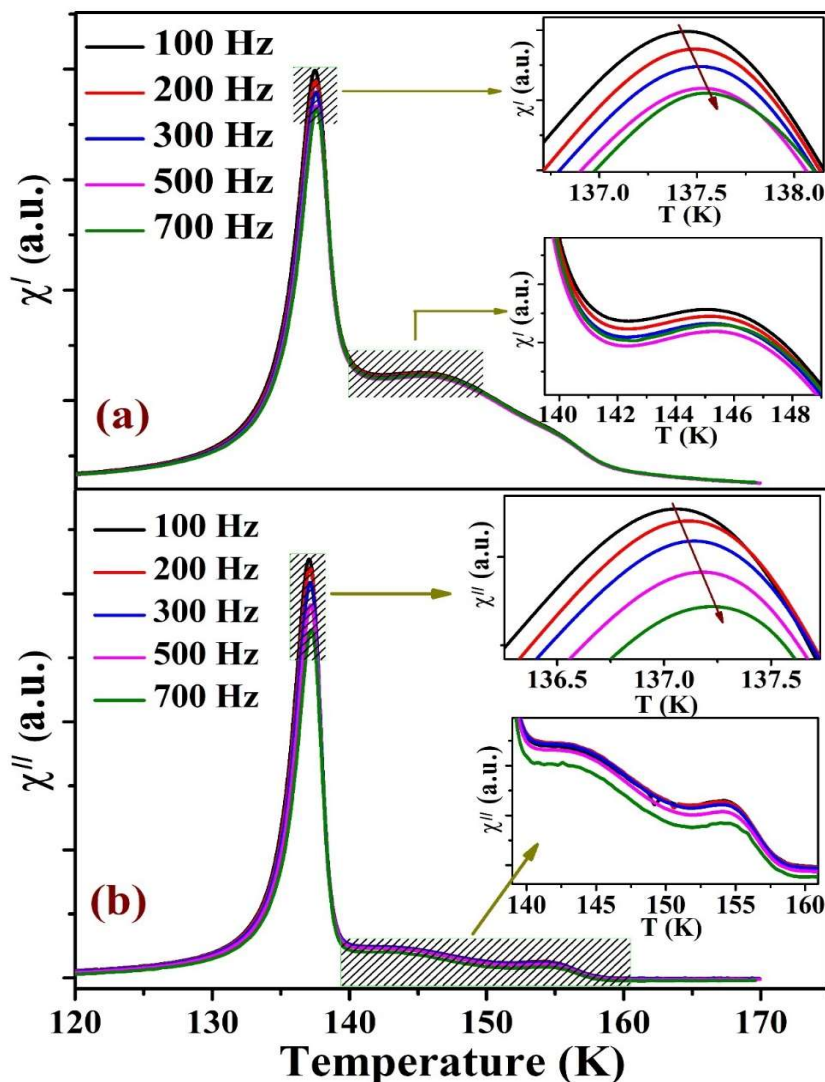
Figure 5.5*: The thermal variation of (a) real part of ac susceptibility and (b) imaginary part of ac susceptibility at different frequency without DC bias around long range magnetic transition region.*
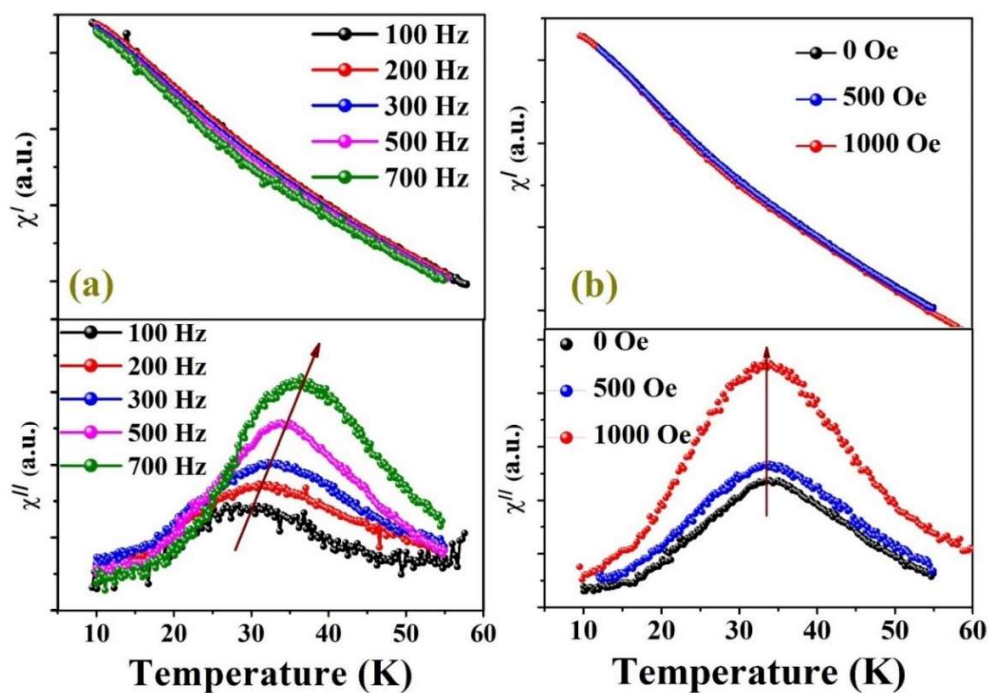
AC susceptibility (χ') and the imaginary part (χ'') of EPCMO shows a clear, frequency-independent peaks near the first magnetic transition T_{C1}, which is attributed to the commencement of long rang magnetic ordering (Fig. 5.5(a, b)). However, near T_{C2}, AC susceptibility shows strong peaks and these peaks show minor shifts towards higher temperature at higher frequencies. Such behavior in the magnetic systems having

miscellaneous interactions is categorized by an arbitrary and cooperative freezing of spins around a defined temperature i.e., the glass temperature (T_g). Beneath T_g, the system enters a region where spin gets frozen with an irregular long-range magnetic ordered state, which is eventually a SG state [259]. As already mentioned, the most important component of spin glass is the presence of different competing exchange interactions and ASD. The calculated value of the parameter p ~ 0.002, where p is defined in terms of peak temperature T_f at frequency f as [256],

$$ p = \frac{\Delta T_f}{T_f \Delta log_{10}(f)} \tag{5.3} $$

Where, p has values between 0.005 to 0.08 for SG or CSG, while for SPM, it should be greater than 0.2. Rather small value of p for our system might be due to weak freezing of spins and the observed peaks is associated with long rang magnetic transition around T_{C2}, as peak shifting is much smaller. It can be mentioned here that the higher temperature spin ordering is disturbed by thermal fluctuations, i.e., the spins are effectively independent of each other [259]. However, at lower temperatures, the spins start communications and form locally frozen units/clusters/droplets/domains. In EPCMO, another broad peak in $\chi''(T)$ curves at lower temperatures below 40 K has been observed (Fig. 5.6(a)). It is the temperature (T_{C3}) where higher field ZFC-M curves show third anomalous magnetic transition. These peaks show a significant shift towards higher temperatures at a higher frequency. For these peaks, the value of the p was found to be around 0.02. Thus, suggesting a re-entrant glassy state in the system [228]. Under application of the DC magnetic field (~1000 Oe) these peaks grow up (Fig. 5.6(b)). Interestingly, the anomaly in DC-magnetization also was observed at higher field. Moreover, as already been described ferromagnetic characteristics exist at lower temperature.

So the emergence of glassy state must be correlated to FM state. Thus, it can be said that there

are clusters of spins in glassy state, forming due to short-range FM ordering within the cluster.

FM cluster-glass phase has also been seen in other systems [260,261].

Figure 5.6: *(a) The thermal variation of real and imaginary part of ac susceptibility at different frequency without DC bias. (b) The thermal variation of real and imaginary part of ac susceptibility at 500 Hz frequency with different DC bias around 40 K.*

5.3.3 Transport properties

Fig. 5.7 shows the variation of the field independent DC resistivity (ρ) with temperature

in the temperature range 60-300 K. This resistivity curve shows the semiconducting/insulating

behavior of the sample. The large value of resistivity might be attributed to the structural

distortion which narrowed 3d-bands and put off the electron hopping [212]. Below 160 K, the

resistivity is best described by the variable range hopping (VRH) model, given by equations

[19–21].

136

$$ln\rho = ln\rho_0 + T_0^{1/4}.T^{-1/4} \qquad (5.4)$$

Where, ρ_0 is a pre-factor. and T_0 is an important parameter; known as Mott's characteristics temperature which is linked with the density of localized states ($N(E_F)$) near Fermi level as,

$$T_0 = 24\alpha^3/\pi k_B N(E_F) \qquad (5.5)$$

The localization length $1/\alpha$ is the average spacing between adjacent Co or Mn ions which is around twice of the Co-Mn bond length [22]. The polaron activation energy (W) at temperature T is $W = 0.25\ k_B T_0^{0.25} T^{0.75}$ with most probable hopping distance,

$$R = \left[\frac{9}{8\pi\alpha k_B N(E_F)}\right]^{1/4} = \left[\frac{9T_0}{192\alpha^4}\right]^{1/4} \qquad (5.6)$$
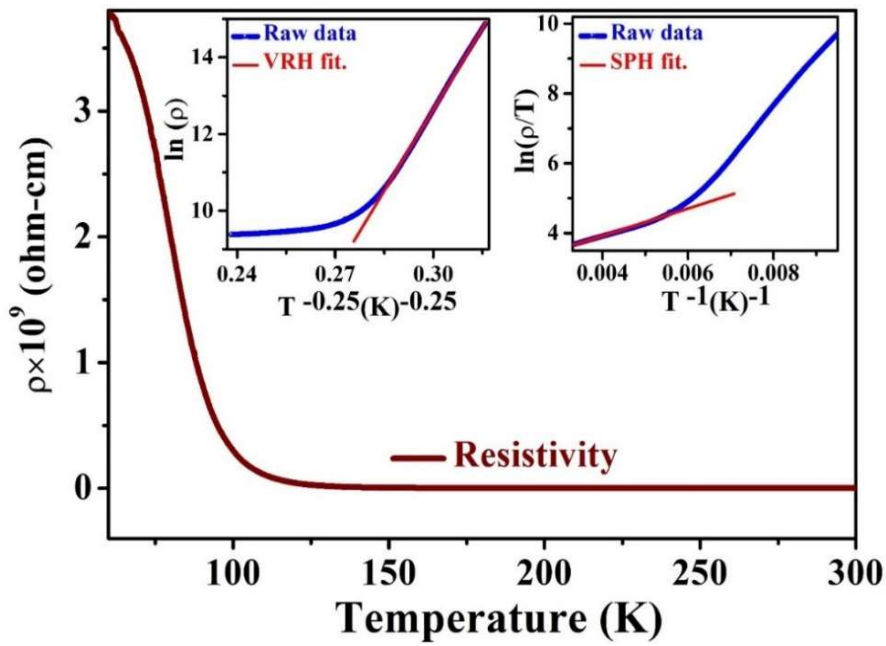
Figure 5.7: *The temperature-dependent resistivity of EPCMO with insets showing VRH and SPH fitting.*
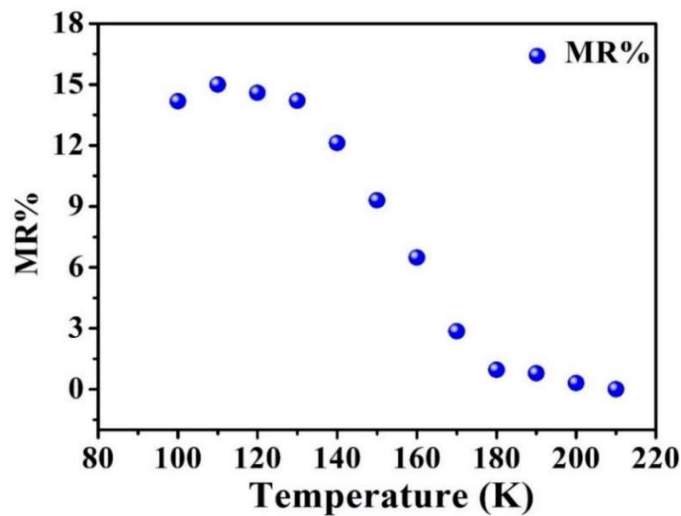
Figure 5.8: *The thermal variations of magnetoresistance at 11 kOe magnetic field of EPCMO.*

The value of N(E$_F$) for EPCMO was found to be ~10^{24} eV^{-1}m^{-3}, which is the order of typical semiconductor materials. The estimated activation energy is larger than thermal energy (k$_B$T) within the investigated temperature range with αR > 1. In this temperature region, the charge carriers are trapped and distributed in a localized narrow band with multiple activation energies and only those electrons will participate in conduction that lies close to the Fermi level. However, in higher temperature region, the trapped carriers hop out so the conduction is governed by some thermally activated mechanism. In the temperature range 160-300 K range our resistivity data is best fitted by small polaron hopping (SPH), given by equation $\rho = \rho_0 T exp\ (E_a/k_B T)$, which is a short-range thermally activated energy process credited to the increased drift mobility and hopping frequency of the charge carriers at higher temperature [227]. The obtained polaron activation energy E$_a$ from SPH fitting is 0.0336 eV. Furthermore, we have observed an increase in resistivity under application of magnetic field below 170 K. Thus, the existence of positive magneto-resistance (MR) has been inferred in EPCMO. The

variation of MR with temperature is shown in Fig. 5.8, under the application of 1.1 kOe magnetic field. On lowering temperature, the MR increases. It is interesting to observe the magnetic ordering emerges in the same temperature region. Thus, it can be understood that the detected MR is associated with coexistence of FM and AFM in the EPCMO.

5.3.4 Dielectric study

The relative dielectric permittivity (ε) and tanδ vs. temperature curves of EPCMO at different frequencies have been demonstrated in Fig. 5.9 with the inset showing dissipation factor (tanδ). The ε-T curve shows almost non-dispersive intrinsic polarization and a low value of ε at low temperature below 150 K due to freezing of dipoles. Beyond 150 K, ε shows step-like increasing behavior and the steps shift towards higher temperature at higher frequency showing a thermally activated polarization. The electrically mixed microstructure i.e., conducting regions owing to ASD and insulating regions as a result of perfect Co/Mn ordering as well as heterogeneity and defects near grain boundary due to Eu/Pr sub-lattices, might be playing a role behind the high value of ε [233]. The heterogeneity increases the probability of inter-well hopping which affects dielectric relaxation mostly at lower frequency and owing to the heterogeneous distribution charge carriers pileup which responds in a different way to the external electric field [234]. These dielectric relaxations are mainly described by non-Debye/Maxwell-Wagner (MW) interfacial polarization where the system does not have a permanent dipole moment [262]. The MW effect takes account of the interfaced depletion layers between sample and contact and at grain boundaries as well [229,231,232]. In this picture, grain (G) and grain boundary (GB) both has their characteristic resistance (R_g & R_{gb}) and capacitance (C_g and C_{gb}) in the heterogeneous polycrystalline sample. To explain our

dielectric relaxation, we have performed the simultaneous impedance measurements for better investigation of grain and grain boundary contributions discussed below.
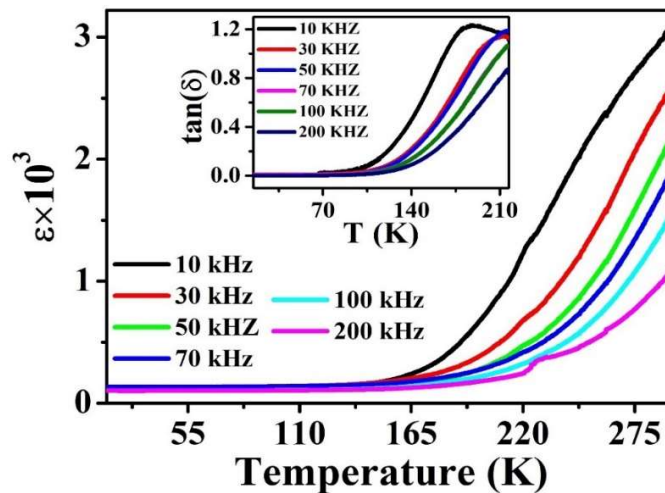
Figure 5.9: *The thermal variations of relative dielectric permittivity of EPCMO with inset showing the thermal variations of dielectric loss at different frequency.*

5.3.5 Impedance spectroscopy

The plot of frequency dependence of the imaginary part (Z″) of the impedance at a few temperatures has been presented in Fig. 5.10. We observed two prominent relaxation peaks (shown with an arrow). These peak shifts towards higher frequencies with decreased intensity as the temperature increases, again implying both electrical responses are thermally activated. Usually complex impedance plots (Z″ *vs.* Z′) i.e., cole-cole plot results in two semi-circular arcs are attributed to each relaxation peak in Z″ [263]. The electrical responses of these peaks are attributed to grain boundary (lower frequency side peak) and grain (higher frequency side peak) conduction [58]. The intensities of the relaxation peaks are proportional to the resistances of grain boundaries and grains respectively. The impedance curves usually are treated as an
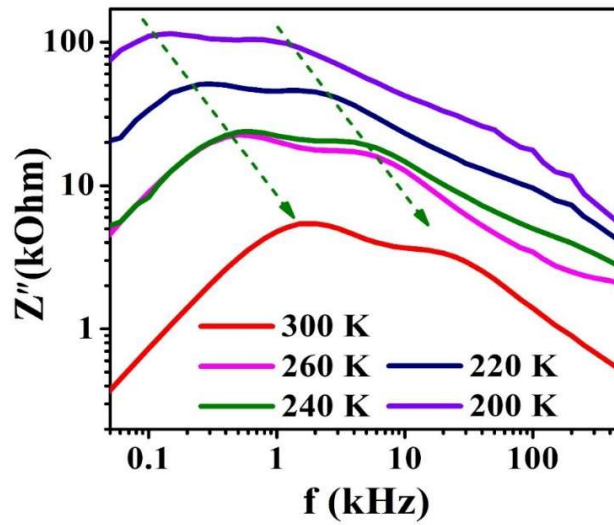
Figure 5.10: *The variation of Z″ with frequency at different temperatures.*

ideal equivalent circuit composed of a resistor R and a capacitor C [263]. Generally, a polycrystalline sample has consisted the intergranular and grain-boundary impedances. Therefore, they can be expressed as an equivalent circuit, consisting of a series of two sub-circuits that take account of grain/grain boundaries effects. Thus, the overall impedance circuit within the system is the result of a series combination of two parallel-connected resistance and capacitance arising from the grain and grain boundary contributions. Accordingly, the $Z″$-dispersion relation can be written as,

$$Z'' = R_g \left[\frac{2\pi R_g C_g}{1+\left(2\pi R_g C_g\right)^2} \right] + R_{gb} \left[\frac{2\pi R_{gb} C_{gb}}{1+\left(2\pi R_{gb} C_{gb}\right)^2} \right] \tag{5.7}$$

And the corresponding grains and grain boundaries response peaks are positioned at frequencies $f = 1/2\pi R_g C_g$ and $1/2\pi R_{gb} C_{gb}$ respectively and peak intensity is equal to $R_g/2$ and $R_{gb}/2$ [262,263]. Using these conditions $R_g, R_{gb}, C_g \ and \ C_{gb}$ has been estimated for our system, shown in Fig 5.11 (a-d).
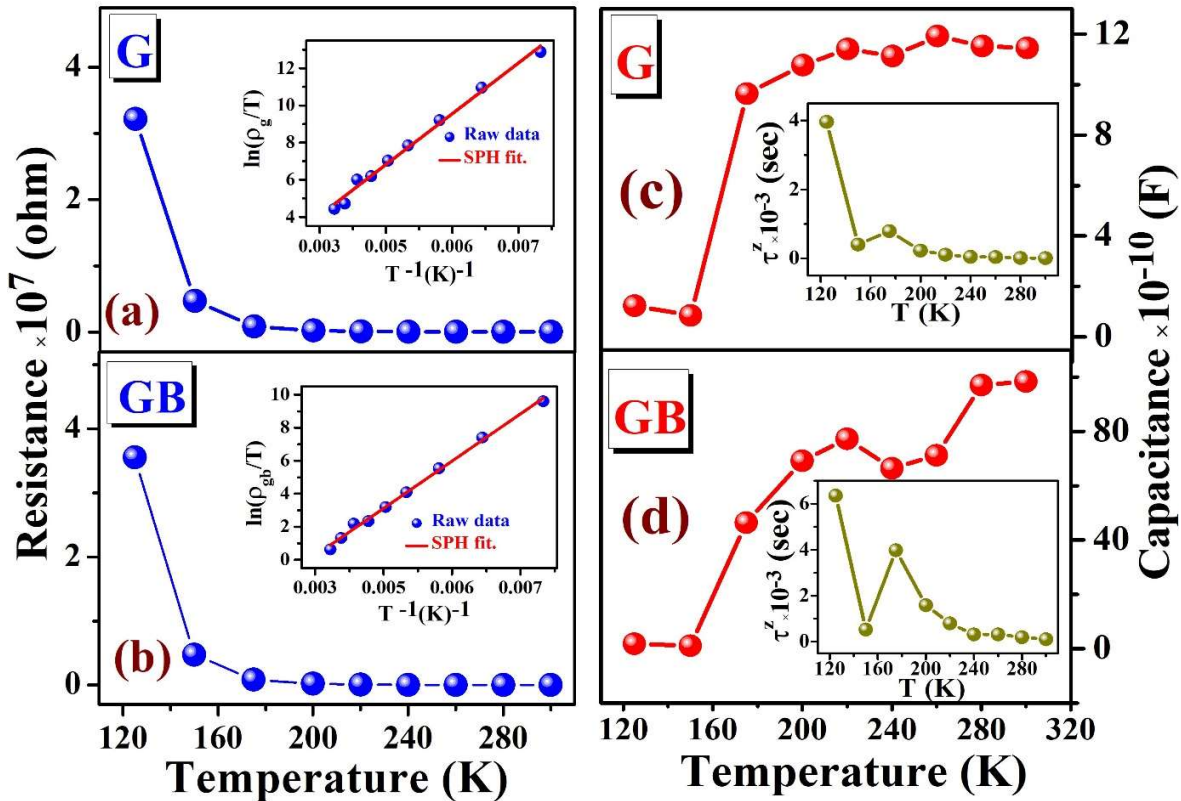
Figure 5.11: *The variation of (a) grain (G) resistance, (b) grain boundary (GB) resistance, (c) grain capacitance and (d) grain boundary capacitance with temperature. The inset of (a & b) shows the SPH fitting of grain and grain resistances (c & d) shows the corresponding response time vs T plot.*

Generally, the conduction mechanism in semiconductor is governed by thermally activated electrons and resistivity varies as $\rho(T) = \rho_0 exp(E_a/k_B T)$. However, in EPCMO the grain and grain boundary resistivity is best fitted by short-range thermally activated small polaron hopping mechanism (shown in the inset of Fig. 5.11 (a, b)), where both grain and grain boundary resistivity follows $\rho(T) = \rho_0 T exp(E_a/k_B T)$, similar to DC resistivity as discussed earlier in this report. Further estimated response time, $\tau^z = R_g C_g \; or \; R_{gb} C_{gb}$ for grain and grain boundary respectively are shown in the inset of Fig 5.11 (c, d). The real part of permittivity can be better explain here seeing that the $R_g < R_{gb}$ and $C_g << C_{gb}$. For the case

142

relatively poorly conducting thinner grain boundaries are separated by lower resistive grains and application of external electric field accumulates localized charge at the interface, thus leads to interfacial MW polarization [264,265]. The response time τ^z increases slowing on decreasing temperature, however below ~150 K, there is sudden increase in τ^z. This is consistent as we have observed a step-like decrease in the real part of permittivity down to ~150 K. Moreover, at higher frequencies, the value of ε′ decreases due to arising of difficulties to follow the applied ac electric signal beyond a certain frequency by hopping frequency of the charges. This process leads to decrease in interfacial polarization [262].

5.4 Conclusion

The detailed structural, magnetic and electrical properties of double perovskite EuPrCoMnO$_6$ have been investigated. The structural analysis shows that the EuPrCoMnO$_6$ crystallizes in a pure single orthorhombic phase with space group *Pnma*. The DC magnetization shows increase in magnetization below 160 K and it exhibits two consecutive long range magnetic transitions around 146 K and 138 K. Further magnetization curve shows a magnetic anomaly around 40 K. Using AC susceptibility measurement, it was proved that this magnetic anomaly was associated with a re-entrant glassy dynamic. A weak glassy dynamic near magnetic transition also was observed in the AC susceptibility spectrum. The inverse DC susceptibility shows a downturn in the paramagnetic region which was eventually associated with Griffiths-like phase. More interestingly, the isothermal magnetization exhibits a metamagnetic transition and asymmetricity around origin at low temperature, showing spontaneous exchange bias in the system. The variation of resistivity with temperature follows VRH and SPH mechanisms. It was also seen that the resistivity increases under application of

DC magnetic field, thus $EuPrCoMnO_6$ shows the appearance of positive magnetoresistance. The dielectric spectrum exhibits frequency-dependent thermally activated steps associated with MW interfacial polarization. Moreover, the contribution of grain and grain boundary in electrical property is observed using the complex impedance study. Overall, owing to large magnetoresistance and high dielectric constant, $EuPrCoMnO_6$ can be a good candidate for spintronic devices and high dielectric applications.